Oxygen Self-Diffusion in HfO_2 Studied by Electron Spectroscopy

M. Vos,[1,*] P. L. Grande,[2,3,†] D. K. Venkatachalam,[2] S. K. Nandi,[2,4,5] and R. G. Elliman[2]
[1]*Atomic and Molecular Physics Laboratories, Research School of Physics and Engineering, The Australian National University, Canberra, Australian Capital Territory 0200, Australia*
[2]*Department of Electronic Materials Engineering, Research School of Physics and Engineering, The Australian National University, Canberra, Australian Capital Territory 0200, Australia*
[3]*Instituto de Física, Universidade Federal do Rio Grande do Sul, 91501-970 Porto Alegre, Rio Grande do Sul, Brazil*
[4]*Research School of Astronomy and Astrophysics, The Australian National University, Canberra, Australian Capital Territory 2611, Australia*
[5]*Department of Physics, University of Chittagong, Chittagong 4331, Bangladesh*
(Received 4 February 2014; published 30 April 2014)

High-resolution measurement of the energy of electrons backscattered from oxygen atoms makes it possible to distinguish between ^{18}O and ^{16}O isotopes as the energy of elastically scattered electrons depends on the mass of the scattering atom. Here we show that this approach is suitable for measuring oxygen self-diffusion in HfO_2 using a $Hf^{16}O_2(20\ nm)/Hf^{18}O_2$ bilayers (60 nm). The mean depth probed (for which the total path length equals the inelastic mean free path) is either 5 or 15 nm in our experiment, depending on the geometry used. Before annealing, the elastic peak from O is thus mainly due to electrons scattered from ^{16}O in the outer layer, while after annealing the signal from ^{18}O increases due to diffusion from the underlying $Hf^{18}O_2$ layer. For high annealing temperatures the observed interdiffusion is consistent with an activation energy of 1 eV, but at lower temperatures interdiffusion decreases with increasing annealing time. We interpret this to be a consequence of defects, present in the layers early on and enhancing the oxygen diffusivity, disappearing during the annealing process.

DOI: 10.1103/PhysRevLett.112.175901 PACS numbers: 66.30.Pa, 68.49.Jk

Self-diffusion is an important but difficult to study phenomenon [1]. Even for silicon, probably the best studied and understood material, the topic of self-diffusion remains an active field of research [2]. There are few options for measuring self-diffusion, with most studies relying on the use of radioactive or low natural abundance isotopes. Analysis is then typically performed with secondary ion mass spectroscopy or other ion-beam based techniques [nuclear reaction analysis, Rutherford backscattering spectrometry (RBS), or the related medium-energy ion-scattering technique].

Oxygen diffusion in HfO_2 and $HfSiO_x$ alloys is of particular interest, as they are being used to replace SiO_2 as the gate dielectric in integrated circuits and are of interest for the fabrication of resistive random access memories based on resistive switching. However, even for pure hafnia, there is little experimental data on oxygen diffusion. Some insight was obtained by monitoring the uptake of ^{18}O after annealing hafnia in a $^{18}O_2$ atmosphere [3,4], but these results depend on oxygen exchange between the sample and O_2 molecules in the ambient, as well as O interdiffusion. Diffusion studies in thin hafnia films (10–20 nm) are made more difficult by the need to resolve small diffusion lengths (1–10 nm). Conventional ion-beam techniques are capable of such resolution but require particular care to ensure that radiation damage does not contribute to the measurement.

Here we address these limitations by employing a novel electron-scattering technique to measure interdiffusion in $Hf^{18}O_2/Hf^{16}O_2$ bilayers. For the energies used, the recoil energy losses are too small to create defects and radiolysis (sample decomposition by electronic excitations) is not important at the modest current densities ($25\ \mu A/cm^2$) employed [5,6]. The consistency of the results indicates that reliable diffusivity data can be obtained from this technique.

HfO_2 layers were grown by atomic layer deposition (ALD) using alternate pulses of tetrakis-(dimethylamido)-hafnium $[Hf(NMe_2)_4]$ and water on a Si substrate heated to 200° C. $Hf^{16}O_2$ films were grown using normal (deionized) water, and $Hf^{18}O_2$ films using water 97% enriched in ^{18}O [7]. Diffusion experiments were performed on $Hf^{18}O_2/Hf^{16}O_2$ bilayers, with layer thicknesses chosen to suit the detection depth of the electron-scattering technique. (i.e., a 20 nm $Hf^{16}O_2$ surface layer grown on a 60 nm $Hf^{18}O_2$ layer). Films of pure $Hf^{16}O_2$ and $Hf^{18}O_2$ were also grown on Si and C substrates to provide reference samples for electron-scattering measurements and to enable independent compositional analysis with RBS. Some samples were annealed for 5 min at temperatures in the range 500–1000° C using a rapid thermal annealing (RTA) system, or for long periods (up to 24 h) at selected temperatures using a conventional silica tube furnace. To prevent oxygen exchange with the ambient, all samples were coated with a 40 nm Si_3N_4 layer prior to annealing. This layer was deposited by plasma enhanced chemical vapor deposition with the substrate at 300° C (2 min), and

 © 2014 American Physical Society

was removed by HF etching prior to analysis. Glancing incidence x-ray diffraction (GI-XRD) analysis confirmed that the as-deposited and Si_3N_4-capped films were amorphous. However, amorphous HfO_2 films are known to crystallize at temperatures above about 400° C, and GI-XRD analysis confirmed that all annealed samples were polycrystalline (monoclinic phase).

If an energetic electron is scattered over a large angle by a nucleus it transfers a significant amount of momentum (q) to this nucleus. As a consequence, the nucleus acquires kinetic energy ($q^2/2M_i$ with M_i the mass of the scattering atom), and the energy of the electron is reduced by this amount. Because of the larger mass of ^{18}O compared to ^{16}O, the energy transfer to ^{18}O is smaller than to ^{16}O. That this is a clearly measurable effect is demonstrated in Fig. 1 for 40 keV electrons scattering from hafnia over 135°. The main elastic peak is due to electrons scattered from Hf, and it is aligned with the energy loss as calculated for an electron scattering from a (free) Hf atom (0.44 eV). A second much weaker peak is expected near 4.86 eV for a hafnia film grown using oxygen with natural abundance and 4.32 eV for a hafnia film grown using ^{18}O atoms. This is indeed the case. The observed peak intensity ratio of the Hf and O peaks are in good agreement with expectations based on calculated elastic-scattering cross sections, which for Hf deviate substantially from the Rutherford values [8,9]. We refer to such an experiment as electron-Rutherford backscattering spectrometry (ERBS) as it is in many ways the electron analogue of (ion) RBS.

If the probing electron transfers momentum $\mathbf{q}$ to an atom with mass M_i and momentum $\mathbf{p}$ before the collision then the recoil energy $E^i_{\rm rec}$ for this atom is given by [10]

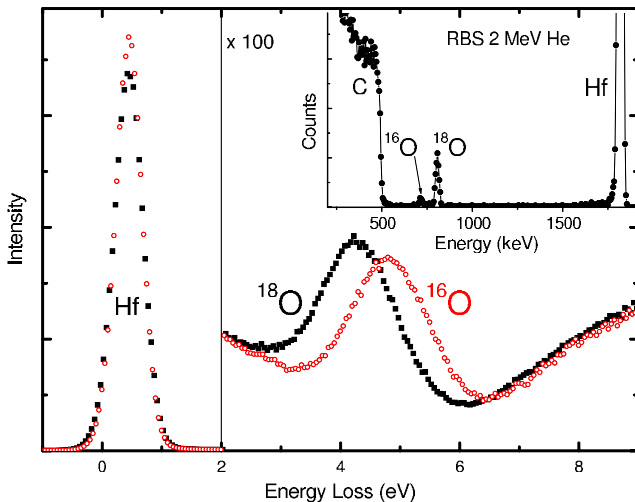

FIG. 1 (color online). ERBS spectra of thick HfO_2 films. The Hf elastic peak is aligned with the calculated recoil energy loss. The O peak position depends clearly on the mass of the isotope used. The inset shows a RBS spectrum that was measured for a HfO_2 film grown on a C substrate with ^{18}O.

$$E^i_{\rm rec} = \frac{(\mathbf{p}+\mathbf{q})^2}{2M_i} - \frac{\mathbf{p}^2}{2M_i} = \frac{\mathbf{q}^2}{2M_i} + \frac{\mathbf{p}\cdot\mathbf{q}}{M_i}. \tag{1}$$

The recoil peak is thus at the energy loss calculated for scattering from a stationary atom, but Doppler broadened due to the motion of the vibrating atoms.

The widths of the ERBS oxygen peaks in Fig. 1 are larger than the width of the Hf peak. The width of each O peak is almost completely intrinsic, i.e., due to Doppler broadening. The Hf peak width is attributed to similar contributions from the energy resolution (here 0.3 eV) and Doppler broadening. Under these conditions an energy resolution better than 1 eV is required to separate the O peak from the (intense) Hf peak.

The momentum distribution of the O atom is taken to be Gaussian (as for the momentum distribution of a harmonic oscillator) and for isotropic systems it can be shown that the width (σ_i) of this Gaussian is related to the mean kinetic energy of the atom [11],

$$\sigma_i = \sqrt{\frac{4}{3}\overline{E^i_{\rm rec}}\,\overline{E^i_{\rm kin}}}, \tag{2}$$

with $\overline{E^i_{\rm rec}}$ the recoil energy for scattering from a stationary atom. The spectra were best described using $\overline{E_{\rm kin}} = 63$ meV. The ERBS spectra of $Hf^{16}O_2$ and $Hf^{18}O_2$ can thus be described with the same formula, using the different masses of the O atoms. The obtained Hf-to-O area ratio is the same for both $Hf^{18}O_2$ and $Hf^{16}O_2$ films.

The inset in Fig. 1 shows the RBS spectrum of a 60 nm $Hf^{18}O_2$ film grown on carbon. Carbon was required since for a Si substrate the O peaks would be on a large "background" due to particles scattered from Si at larger depths, thus complicating the analysis. The spectrum shows that the film was indeed heavily enriched in ^{18}O but the observed ^{16}O presence (≈ 10%) was somewhat larger than in the starting material. The presence of a small amount of ^{16}O in the $Hf^{18}O_2$ layer was included in the model calculations used.

Oxygen self-diffusion was investigated by monitoring the redistribution of $^{16}O_2$ and $^{18}O_2$ in the sandwich structure described above. The oxygen part of the ERBS spectrum, after RTA at the temperatures indicated, is shown in Fig. 2. There is a systematic movement of the maximum of the peak to lower energy losses with increasing annealing temperature. This is due to ^{18}O moving from the underlying $H^{18}O_2$ film towards the surface. The inelastic mean free path λ of 40 keV electrons in hafnia is ≈ 35 nm [12]. Even for the bulk sensitive geometry [incoming beam $\theta_{\rm in} = 0$ (along surface normal), outgoing beam $\theta_{\rm out} = 45°$] the majority of events contributing to the elastic peak occur in the outermost 20 nm. A second set of spectra was obtained in a surface-sensitive geometry ($\theta_{\rm in} = 35°$, $\theta_{\rm out} = 80°$), and are shown in Fig. 2(b). Here, virtually all events contributing to the elastic peak occur in the outer 20 nm.

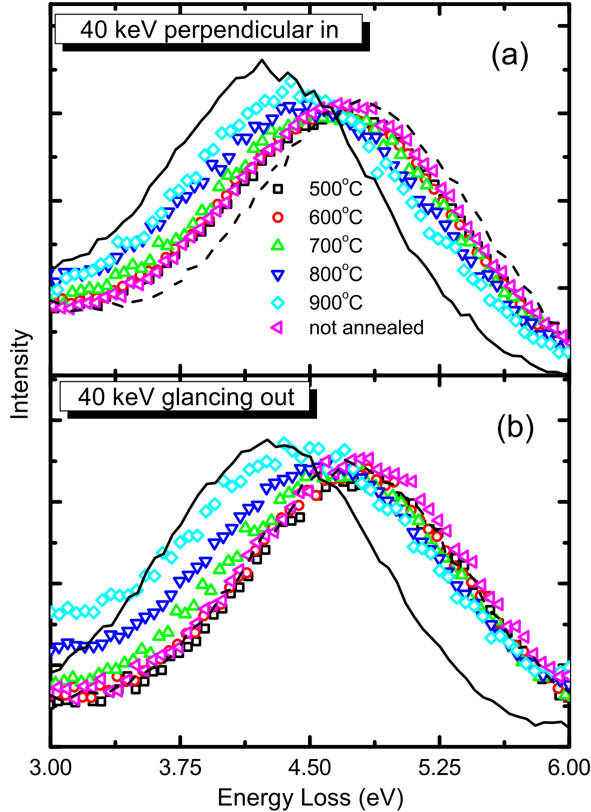

FIG. 2 (color online). The ERBS spectra corresponding to the O elastic peak for a sandwich structure (20 nm $Hf^{16}O_2$ grown on top of 60 nm $Hf^{18}O_2$) after 5 min RTA annealing at the temperatures indicated. The full and dashed lines correspond to the isotropically pure spectra shown in Fig. 1. (a) Shows results for a bulk-sensitive measurement geometry and (b) for a surface-sensitive geometry.

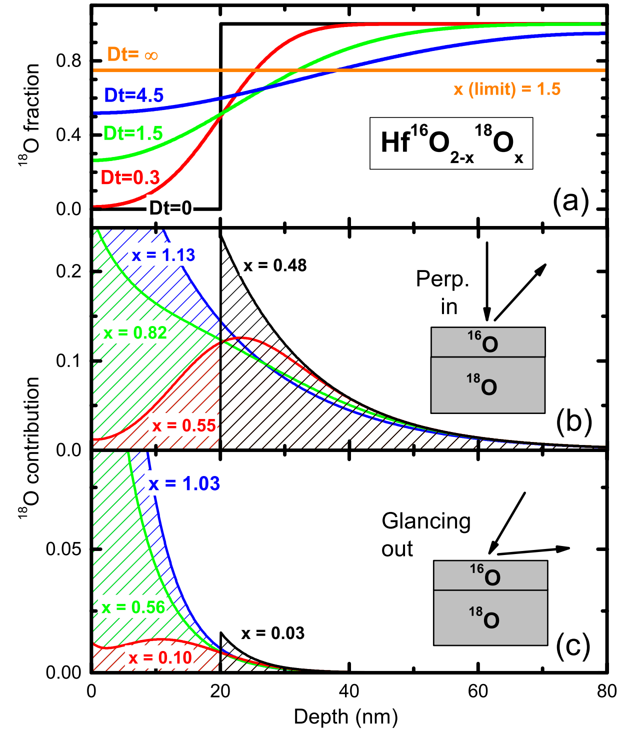

FIG. 3 (color online). The top panel shows the ^{18}O concentration after diffusion by Dt amounts (in units of 10^{-12} cm^2), as indicated. The lower panels show, for both experimental geometries, the probability that ^{18}O contributes to the elastic peak for these Dt values (i.e., the concentration of ^{18}O at that depth times the attenuation due to inelastic scattering along the incoming and outgoing paths). Each curve is labeled with the depth-averaged stoichiometry, as expected for ^{18}O for these diffusion profiles.

We now fit the spectra in Fig. 2 as linear combinations of $Hf^{18}O_2$ and $Hf^{16}O_2$ spectra with the parameters, as determined from the measurements in Fig. 1, kept fixed. These spectra can then be characterized as a $Hf^{16}O_{2-x}{}^{18}O_x$ spectrum where x is determined by the effective amount of ^{18}O probed in a specific geometry. The obtained x value reveals the amount of oxygen diffusion as explained next.

Figure 3(a) shows the ^{18}O distribution as a function of Dt, where D is the diffusion coefficient and t the annealing time. For each concentration profile we calculate the probability of measuring an electron scattered at depth z from an ^{18}O atom. This probability is proportional to the concentration of ^{18}O at depth z *and* an attenuation factor. This attenuation factor describes the likelihood that no inelastic event occurred along either the incoming or outgoing trajectory and is given by $e^{-L/\lambda}$ with L the total path length ($L = z/\cos\theta_{\rm in} + z/\cos\theta_{\rm out}$). This assumes that trajectories are V shaped; i.e., there is only one large-angle deflection. This is a good approximation at these energies as can be seen by extrapolating the results of Ref. [13] to 40 keV.

The ^{16}O signal is calculated identically but now the concentration of ^{16}O is taken to be 2 minus the concentration of ^{18}O. From the ratio of the depth-integrated intensity of the ^{18}O signal [i.e., the area under the curves in Figs. 3(b) and 3(c)] and the ^{16}O signal, we obtain the effective x value as indicated in Fig. 3. This x value is compared with the one extracted from the ratio of ^{16}O and ^{18}O required to fit the oxygen elastic peak. Figure 4 summarizes the relation between x and Dt for both geometries and the x values obtained in the two geometries are consistent with the same Dt value.

The diffusion length (defined as $\sqrt{Dt}$) corresponding to the Dt values describing the different samples are shown in Fig. 5(a). The dashed line is proportional to the expected diffusion length (for a constant anneal time) assuming $D = D_0 e^{-E_{\rm act}/kT}$ with $E_{\rm act} = 1$ eV. At first sight this appears to fit the experimental data reasonably well. However, at the lower temperatures, where conventional annealing experiments were also done, the diffusion length is found to increase much more slowly with annealing time than expected for a $\sqrt{Dt}$ dependence. This means that the diffusivity D decreases with time during the anneal treatment. These observations are clearer when D is plotted as

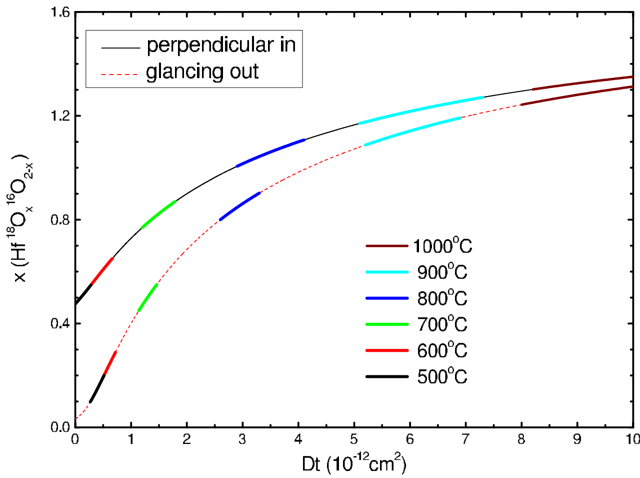

FIG. 4 (color online). The effective concentration of ^{18}O for the perpendicular in geometry (solid line) and glancing out geometry (dashed line)as a function of Dt. The range of x values consistent with the measurement after RTA annealing at the temperatures indicated are superimposed on this line. In this way the Dt value for each annealing temperature can be read from the horizontal axis.

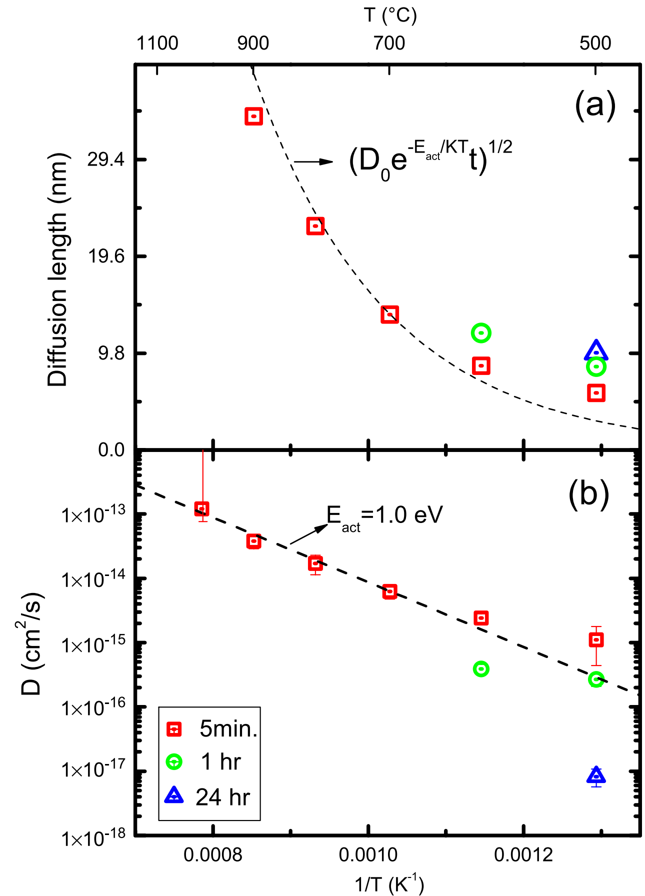

FIG. 5 (color online). (a) The diffusion length ($\sqrt{Dt}$), derived from fitting the ERBS spectra with a ^{18}O and a ^{16}O elastic peak, and the concentration profiles shown in Fig. 3. At lower temperatures several experiments were done with annealing times as indicated. The obtained diffusion lengths increased only slightly with annealing times. In (b) we show the obtained D values which decrease with increasing annealing times. The dashed line is proportional to the expected D values and diffusion lengths for an activation energy of 1 eV. These values do not describe the RTA experiment perfectly.

an Arrhenius plot, as in the lower panel of Fig. 5. For the higher temperature measurements, an activation energy of 1 eV describes the temperature dependence of D reasonably well considering the larger error bars for the lower temperature measurements. But with increasing anneal time the diffusivity at low annealing temperatures drops by 2 orders of magnitude.

It is tempting to explain this in terms of an initial rapid diffusion associated with relaxation and crystallization of the amorphous film, followed by slower diffusion in the crystalline film. This hypothesis is reasonable as relaxation in disordered systems is often time dependent. The diffusivity can thus be initially larger than the diffusivity for a well-annealed sample. The excess diffusivity Δ reduces during the annealing step and this reduction is commonly described by a stretched exponential: $\Delta \sim \exp -[(t/\tau)^{\beta}]$ [14]. However, comparison of the data for 1 and 24 h anneals at 500° C shows that D continues to decrease with time, even though GI-XRD analysis shows that the film is polycrystalline after 5 min at 500° C.

Diffusion in HfO_2 is complicated due to the different possible charge states of both the O vacancy and O interstitials, and the roles of crystallization and grain boundaries. As a consequence, there are very few reports of measured self-diffusion coefficients. Clima *et al.* calculated values between 0.57 and 0.66 eV for the activation energy for substoichiometric films [15] and Capron obtained values of 0.7 and 2.4 V eV for the activation energy of positively charged and neutral vacancies, respectively, in monoclinic HfO_2 [16]. Rather indirect experimental evidence of Zafar *et al.* based on measured transient gate currents give values between 0.46–0.60 eV.

In the present context, it is interesting that the activation energy of 1 eV that seems to fit the higher temperature data, is consistent with values employed in models of diffusion in resistive random access memory structures [17,18] and determined by theoretical means (e.g., [19,20]). While this is encouraging, it is clear that the current experiments go only part way to addressing diffusion in HfO_2 and a detailed understanding is still a difficult task ahead.

In summary, we have shown that ERBS can distinguish oxygen isotopes present in relatively shallow oxide layers (10 s of nm) and hence can be used to study oxygen diffusion. We subsequently used ERBS to monitor interdiffusion in $Hf^{18}O_2/Hf^{16}O_2$ bilayers. The measured RTA diffusion data were consistent with oxygen having an activation energy for self-diffusion near 1 eV at temperatures above 700° C. At lower temperatures the diffusivity

decreases significantly with time, indicating that more than one mechanism is operative.

This work was made possible by funding of the Australian Research Council. P. L. G. acknowledges the Brazilian agency CAPES (Proc. 102209/12-3) for financial support. We are indebted to Kidane Belay for the Si_3N_4 deposition and etching.

*Maarten.Vos@anu.edu.au
†grande@if.ufrgs.br

[1] G. E. Murch, *Phase Transformations in Materials* (Wiley-VCH Verlag GmbH, New York, 2001), Chap. 3.
[2] H. Bracht, H. H. Silvestri, I. D. Sharp, and E. E. Haller, Phys. Rev. B **75**, 035211 (2007).
[3] L. V. Goncharova, M. Dalponte, D. G. Starodub, T. Gustafsson, E. Garfunkel, P. S. Lysaght, B. Foran, J. Barnett, and G. Bersuker, Appl. Phys. Lett. **89**, 044108 (2006).
[4] M. Zhao, K. Nakajima, M. Suzuki, K. Kimura, M. Uematsu, K. Torii, S. Kamiyama, Y. Nara, H. Watanabe, K. Shiraishi, T. Chikyow, and K. Yamada, Appl. Phys. Lett. **90**, 133510 (2007).
[5] R. Egerton, P. Li, and M. Malac, Micron **35**, 399 (2004).
[6] M. McCartney, P. Crozier, J. Weiss, and D. J. Smith, Vacuum **42**, 301 (1991).
[7] Supplied by Novachem, see www.novachem.com.
[8] F. Salvat, A. Jablonski, and C. J. Powell, Comput. Phys. Commun. **165**, 157 (2005).
[9] P. L. Grande and M. Vos, Phys. Rev. A **88**, 052901 (2013).
[10] M. Went and M. Vos, Nucl. Instrum. Methods Phys. Res., Sect. B **266**, 998 (2008).
[11] M. Vos, R. Moreh, and K. Tőkési, J. Chem. Phys. **135**, 024504 (2011).
[12] S. Tanuma, C. J. Powel, and D. R. Penn, Surf. Interface Anal. **20**, 77 (1993).
[13] A. Jablonski and C. Powell, Surf. Sci. **551**, 106 (2004).
[14] J. Kakalios, R. A. Street, and W. B. Jackson, Phys. Rev. Lett. **59**, 1037 (1987).
[15] S. Clima, Y. Y. Chen, R. Degraeve, M. Mees, K. Sankaran, B. Govoreanu, M. Jurczak, S. De Gendt, and G. Pourtois, Appl. Phys. Lett. **100**, 133102 (2012).
[16] N. Capron, P. Broqvist, and A. Pasquarello, Appl. Phys. Lett. **91**, 192905 (2007).
[17] D. Ielmini, IEEE Trans. Electron Devices **58**, 4309 (2011).
[18] S. Larentis, F. Nardi, S. Balatti, D. C. Gilmer, and D. Ielmini, IEEE Trans. Electron Devices **59**, 2468 (2012).
[19] A. S. Foster, A. L. Shluger, and R. M. Nieminen, Phys. Rev. Lett. **89**, 225901 (2002).
[20] A. S. Foster, F. Lopez Gejo, A. L. Shluger, and R. M. Nieminen, Phys. Rev. B **65**, 174117 (2002).